Impact of backscatter material thickness on the depth dose of orthovoltage irradiators for radiobiology research

Quan Chen*[1], Janelle Molloy[1], Tadahide Izumi[2], Daret St Clair[2], Edmond Sterpin[3,4]

[1] Department of Radiation Medicine, The University of Kentucky, Lexington, KY 40536, USA

[2] Department of Toxicology and Cancer Biology, The University of Kentucky, Lexington, KY 40536, USA

[3] KU Leuven, Department of Oncology, Laboratory of Experimental Radiotherapy, Leuven, Belgium

[4]Université catholique de Louvain, Institut de Recherche Expérimentale et Clinique, Center for Molecular Imaging, Radiotherapy and Oncology, Brussels, Belgium

Please send correspondence to:

Quan Chen, Ph.D.

Associate Professor

Radiation Medicine, University of Kentucky

Markey Cancer Center, Rm CC063

800 Rose St.

Lexington, KY 40536-0293

859-323-4967 (w)

qchen@uky.edu

Abstract

Accuracy of the dosimetry in radiation research is very important. The orthovoltage X-Ray energy frequently used in radiation research is prone to suffer from dosimetry errors due to the insufficient backscatter condition. In many radiobiology studies, especially for cell irradiations, sophisticated dose calculation algorithm such as Convolution-Superposition or Monte Carlo is not used and hand calculation is relied on for dose estimation. Having a clear idea for the impact of insufficient backscatter on dosimetry is critical for the correct estimation of the dose. The purpose of this study is to demonstrate the magnitude of this dose error and provide lookup tables to account this issue. The beam spectra of several widely used commercial systems (XRAD-225, XRAD-320, SARRP) were used in Monte Carlo (MC) simulations on a series of phantom setups to investigate the impact of backscatter condition on dosimetry. The depth dose curves for different field sizes, different water phantom thicknesses and different beam qualities were generated. Also produced are depth dependent backscatter factors for different field sizes and different beam qualities. It is demonstrated that as much as 50% dose difference exists for different backscatter conditions at the beam qualities studied. Also, the choice of cell dish size as well as other changes in the experiment setup can have more than 10% impact to the dose. The impact of backscatter is reduced with the decrease of the field size. It is also found that the backscatter thickness needed to provide full backscatter roughly equals to the field size used at the orthovoltage energy studied. It is very important to either ensure the full backscatter condition during system calibration and dosimeter calibration by providing enough backscatter material and use small field size or use a look-up table such as the one provided by this study for correction factors.

Introduction

Radiobiology research aims to establish the relationship between the radiation dose and its biological effect. It has led to many fundamental scientific insights, and continuing to provide rationale for implementation of new treatment strategies. Many biological effects are very sensitive to the radiation dose. It has been demonstrated that a deviation of 3% in target dose can result in 10% change in the tumor control probability (Brahme, 1984). In addition, the responses of many organs at risk are very sensitive to the change in the radiation dose, including spinal cord (Kirkpatrick *et al.*, 2010), lung (Marks *et al.*, 2010; Van Dyk *et al.*, 1981), gastro intestine (Kavanagh *et al.*, 2010), etc. Therefore, it is very important to ensure the accuracy of the dosimetry in radiation research. However, it has been shown that the dosimetry in many radiobiology studies were questionable (Desrosiers *et al.*, 2013). A survey of 4 radiobiology labs showed that dose errors on the order of 20%-40% existed in their experiments (Robbins, 2011). Another survey of the radiation biology irradiator at 12 laboratories showed that only one out of five facilities using X-Ray irradiators delivered dose within 5% of the desired dose (Pedersen *et al.*, 2016). While it is recognized that the contributing reason is the lack of radiation physics training by many biologist, the complexity of the dosimetry at the energy level used in radiobiology research is another important factor. Specifically, for radiobiology studies, due to the thickness of the cell plate and small animals, X-Ray energy of 30-320 kVp is normally used (Yoshizumi *et al.*, 2011). Most dosimeters used clinically were unable to provide correct dose measurement due to the energy response, as shown in a nice overview of common dosimetry systems by Desrosiers et. al. (Desrosiers *et al.*, 2013). It has been recommended (Desrosiers *et al.*, 2013) that the air-filled ionization chambers be used for the calibration due to its flat energy dependence between 50 keV and 200 MeV and the Accredited Dosimetry Calibration Laboratory (ADCL) calibration, as well as many other advantages. The recommended calibration protocol is the AAPM TG-61 report (Ma *et al.*, 2001), which covers the X-ray energy of 40-300 kV.

AAPM TG-61 presented two calibration methods: “in-air” and “in-phantom” method. The “in-phantom” method is only for energy >100 kV while “in-air” method is good for all energies. Briefly, the “in-air” method involve of measuring air-kerma (“dose to air”) at a reference point in air ($K_{air}^{in\text{-}air}$). The values are then converted to water-kerma ($K_{w}^{in\text{-}air}$) by multiplying with ratio of mass energy-absorption coefficients water to air, free in air ($\left[\left(\overline{\mu_{en}}/\rho\right)_{air}^{water}\right]_{air}$). Finally, for dose to water at flat surface at reference point (D_w), the water kerma is multiplied with a backscatter factor (B_w) to account for the effect of backscatter from the material beneath the surface. B_w is field size, beam quality and SSD dependent and TG-61 includes a table of B_w computed through Monte Carlo simulation. B_w can be well over 1.4 for the X-ray energy and SSD commonly used in two popular commercially available radiobiology X-ray irradiators (Xstrahl SARRP and Precision X-RAD)(Wong *et al.*, 2008; Deng *et al.*, 2007; Jaffray, 2007). However, the dose to water at surface obtained assumes there is enough material below the surface to fully build up the back-scatter, which was almost never the case for actual use. Often, the cell plate is placed on a plastic platform of a few millimeters thick. In the case of small animal irradiation, the small animal itself, plus the immobilization device, could provide several centimeters of backscattering material. The backscatter it provides is likely far less than the B_w in TG-61 shows. However, there is no table to provide a better estimate of the dose at surface under those conditions. As a result, the researchers either wrongfully assumes the B_w in TG-61 table applies to their setup, or rely on other dosimeters (such as film, OSLD) to measure the dose for their setup, which brings more uncertainty and defeat the purpose of using the ADCL calibrated ion chamber for calibration.

The “in-phantom” method of the TG-61 suffers similar issue in that the dose at the reference depth is calibrated for the backscatter condition of the calibration setup (usually has enough depth of water phantom to provide full backscatter). For the radiation experiments, using the calibrated dose at reference depth plus the percentage depth dose curve obtained in different setup will bring error in the estimation of dose administered.

Several sophisticated dose calculation engines have been developed, including convolution-superposition based(Jacques *et al.*, 2010; Cho *et al.*, 2018) and Monte Carlo based(Verhaegen *et al.*, 2011; van Hoof *et al.*, 2013; Bazalova *et al.*, 2009). While these dose calculation engines would be able to handle complex scatter conditions, they usually require the input of a volumetric representation of experiment setup. While high-end irradiators focusing on small animal use usually have integrated 3D imaging capability, many irradiator models targeting mainly for cell and tissue irradiation do not have 3D imaging capability. Even on irradiators with imaging capability, the imaging is usually not used for cell irradiation. Thus, in many occasions, dose has to be hand-calculated based on TG-61 calibration result. The correct interpretation of the scatter condition is critical in ensuring the dosimetry accuracy.

The main purposes of this study are to: (1) demonstrate the magnitude of the dose error when the backscatter material is not sufficiently accounted; (2) provide a depth-dose look-up table as well as backscatter factor table at different thickness of water phantom for researchers to use in their hand calculation. In addition, the impact of other materials and conditions in experiment setup, such as the use of cell-dish, stainless steel, low density polyurethane foam will be investigated.

Material and Methods

The PENELOPE Monte Carlo (MC) code (Salvat *et al.*, 2006) is used in this study. PENELOPE is a general-purpose Monte Carlo code system for the simulation of coupled electron-photon transport. It has been widely used and validated in various radiation therapy applications (Verhaegen and Seuntjens, 2003; Sterpin *et al.*, 2013; Sempau *et al.*, 2001), including low and medium energy X-ray (Ye *et al.*, 2004; Chica *et al.*, 2009). Since the present study focuses on the change in phantom backscatter at different phantom thickness, the detailed simulation of the x-ray tube and collimation was omitted. Instead, we assume a point source with the photons' energy sampled from the photon spectra (Figure 1). The XRAD 225 and XRAD320 spectra and half value layer (HVL) values were provided by the manufacturer. The

SARRP spectrum was provided by the original inventors at John Hopkins (Wong *et al.*, 2008) and the HVL value was provided by the manufacturer(Bazalova *et al.*, 2014). The detailed descriptions of the machines and beam qualities simulated in this study are listed in Table 1. For the rest of this paper, we will differentiate the two beam qualities of the XRAD 225 as X225(Cu) and X225(Al) to indicate the filter used.

Table 1 X-ray units and beam qualities studied.

Device	Energy	Added filter	HVL
Precision XRAD 225, Precision X-Ray Inc., North Branford, CT (X225)	225 kVp	0.3 mm Cu	0.92 mm Cu
		2.0 mm Al	0.37 mm Cu
SARRP, XStrahl Inc., Suwanee, GA (SARRP)	220 kVp	0.16 mm Cu	0.66 mm Cu
Precision XRAD 320, Precision X-Ray Inc., North Branford, CT (X320)	320 kVp	Thoraeus (0.8 mm Sn, 0.25 mm Cu, 1.5 mm Al)	3.86 mm Cu

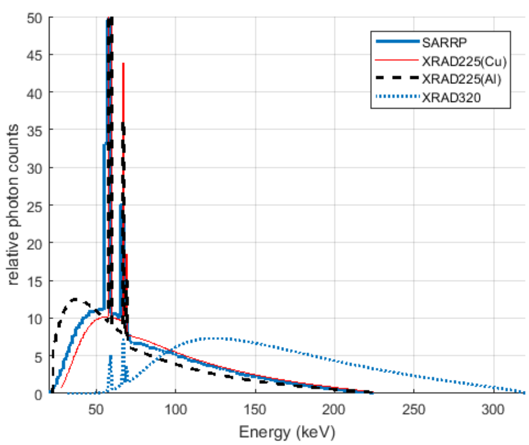

Figure 1. Photon fluence spectra for the X-ray units and beam qualities studied.

Absorbed dose to water at phantom surface is determined according to TG61(Ma *et al.*, 2001) :

$$D_{w,z=0} = MN_k B_w P_{stem,air} \left[\left(\frac{\mu_{en}}{\rho} \right)_{air}^{water} \right]_{air}, \quad (1)$$

where *M* is the free-in-air ion chamber reading; N_k the air-kerma calibration factor for the beam quality; $P_{stem,air}$ the chamber's stem correction factor; B_w the backscatter factor which accounts for the phantom scatter effect; $\left[(\overline{\mu_{en}}/\rho)_{air}^{water}\right]_{air}$ the in-air mass energy absorption coefficient ratios that converts air kerma to water kerma. Using different notation, eq. 1 can be expressed as:

$$D_{w,z=0} = B_w {k_w}^{in-air}, \tag{2}$$

where

$$ {k_w}^{in-air} = \left[\left(\frac{\overline{\mu_{en}}}{\rho}\right)_{air}^{water}\right]_{air} {k_{air}}^{in-air}, \tag{3}$$

and

$$ {k_{air}}^{in-air} = M N_k P_{stem,air} \ . \tag{4}$$

Note that the TG61 assumes there is enough material below the surface to provide full backscatter. The B_w table contains only source to surface distance (SSD), field size and beam quality (in HVL) as variable. In the situation when there is not enough material to provide full backscatter, the backscatter factor will depend on the material thickness (*T*) as well. We hereby define the thickness dependent backscatter factor as ${B_w}'(T)$ and call TG61's B_w as "full backscatter factor". The equation (2) is rewritten as:

$$D_{w,z=0} = B_w^{\prime(T) {k_w}^{in-air}}. \tag{5}$$

Note:

$$B_w = {B_w}'(\infty). \tag{6}$$

Equations 2-4 demonstrates how the dose to water at phantom surface can be inferred from the ion chamber reading in in-air measurement. On the other hand, the $K_{air}^{in\text{-}air}$, $K_w^{in\text{-}air}$, and D_w can all be obtained directly through MC simulation in the geometry illustrated in Figure 2. In Figure 2a setup, the simulation is performed in air, with a voxel right below the isocenter assigned a material of air but a physical density of 1.0 g/cm^3 for better statistical precision of the MC dose. The dose tallied in the voxel is the air kerma $K_{air}^{in\text{-}air}$. Figure 2b is the same as 2a except the material of the tallying voxel become water. The dose tallied in this scenario is the water kerma $K_w^{in\text{-}air}$. In Figure 2c, a water phantom was placed with the top surface at isocenter. The water phantom is 51.2 cm by 51.2 cm with thickness (*T*) of [0.2, 0.4, 0.6, 0.8, 1.6, 2.4, 3.2, 6.4, 12.8, 41.2] cm simulated for our study. The maximum thickness simulated (41.2 cm) was assumed to be sufficient for the full backscatter buildup. The dose tallied at the surface is the surface dose D_w. From these simulation B_w and $\left[(\overline{\mu_{en}}/\rho)_{air}^{water}\right]_{air}$ can be computed following Equations 2-3 and compared with the TG-61 tables. The agreement can serve as a validation of our MC simulation.

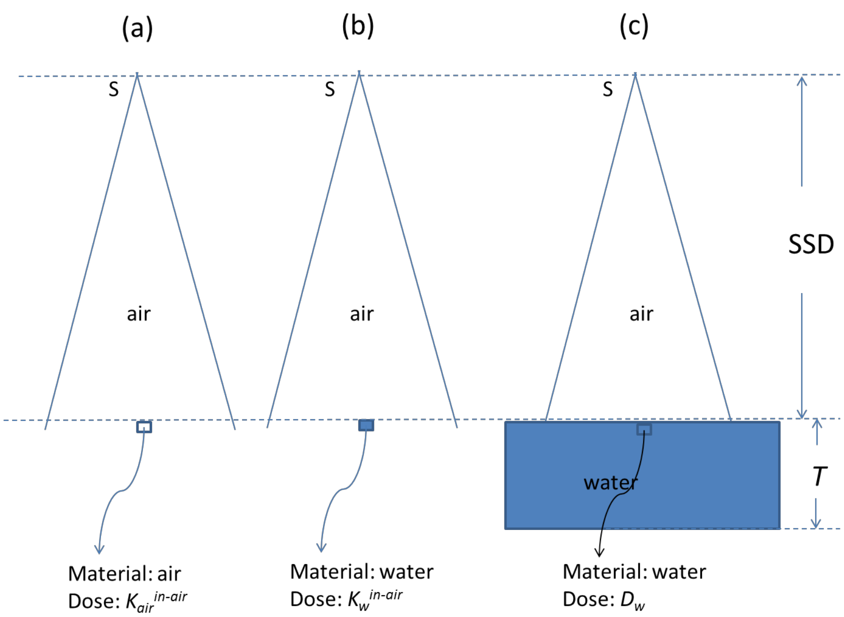

Figure 2. Phantom setups in MC simulations. (a) A voxel with material of air right below the isocenter recorded the dose. (b) The same voxel with material of water recorded the dose. (c) A water phantom was placed with top surface at isocenter. Both the surface dose and the dose profile along the depth direction were recorded.

For Figure 2a and Figure 2b setup, 2e8 photons per cm^2 were simulated. In addition, simulation was repeated 6 times with different random seed and dose in a single 2 mm × 2 mm × 2 mm voxel at isocenter was analyzed to estimate statistical uncertainty. For Figure 2c setup, simulation was not repeated since the statistical uncertainty can be reduced through spatial averaging. To compare with TG61 B_w table, square field sizes of 1, 2, 3, 5, 10, 15, 20 cm were simulated. Note that the TG61 table uses circular aperture diameter for field size. To compare with square field sizes result we multiple the diameter by a factor of $\sqrt{\pi}/2$ to convert them to square field sizes (Podgorsak, 2005). For field size less than 5 cm, 2e8 photons per cm^2 were simulated and depth dose at each 2mm depth increment was obtained by averaging a 6 mm×6 mm region around the beam axis. For field size greater than 5 cm, 2e7 photons per cm^2 were simulated but spatial averaging was performed on 30 mm×30 mm region at each depth. For MC settings, electron cutoff energy of 1 keV and photon cutoff energy of 100 eV were used.

In addition to the standard TG61 calibration geometry, we simulated several scenarios that may be closer to the actual radiobiology experimental setup shown in Figure 3. The setups all involve a 30×30×1.2 cm square water block (simulating the supporting platform) with top surface at the isocenter. The difference is that: (a) another 30×30×1.2 cm square water block was placed on top as a reference; (b) a 1.2 cm thick water cylinder was placed on top to simulate cell dish, with diameter of the dish simulated as 3.5 cm, 6.0 cm and 10.0 cm; (c) same as (a) but with extra 4 mm stainless steel underneath; and (d) same as (a) but with extra 20 cm polyurethane foam with density of 0.03 g/cm^3 underneath. Note that the parameters used in these simulations (material, size and thickness of supporting platform, size and thickness of cell dish, etc.) may not be the same as those used in actual experiment. The purpose of this simulation was to simply illustrate qualitatively the dosimetry impact with each setup. The top of the supporting platform is set at 50cm from the radiation source (dashed line). This put the SSD at 48.8 cm.

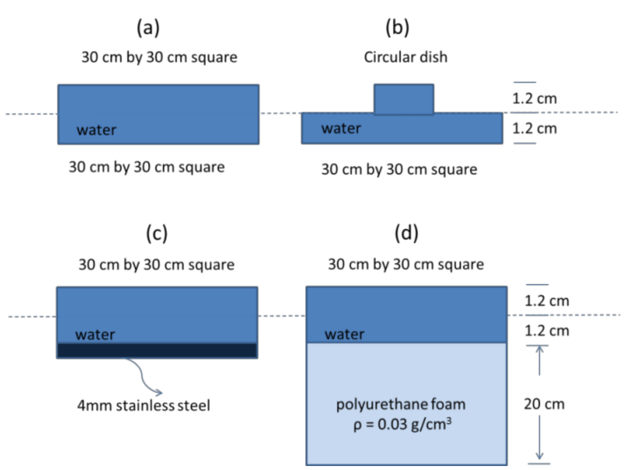

Figure 3. Different phantom setups to investigate the dosimetric impact of changes in phantom setup. (a) Same size of water blocks for reference. (b) Placing a cell dish on top of a supporting board. (c) Put a 4 mm thick stainless steel below the supporting board. (d) Putting a low density polyurethane foam below the supporting board.

Results

The air kerma, water kerma, and surface doses on a 41.2 cm-thick water block were simulated. The statistical uncertainty of air kerma and water kerma were 0.3% for each run and reduced to 0.12% after averaging. The statistical uncertainty for surface doses were <0.1% after spatial averaging. The $\left[(\overline{\mu_{en}}/\rho)_{air}^{water}\right]_{air}$ computed from our MC simulation were in good agreement with TG61 table lookup, as shown in Table 2. The X225(Al) result showed 1.29% deviation, most likely due to the difference between vendor-provided spectrum and the one used to generate the TG61 table.

Table 2. Comparison of the in-air mass energy absorption coefficient ratio from MC-simulation and from TG61 table look-up using the HVL of the beam.

Beam quality	$[(\overline{\mu_{en}}/\rho)_{air}^{water}]_{air}$		
	MC	**TG61**	**Difference**
X225(Cu) HVL: 0.92 mm Cu	1.074	1.072	0.14%
X225(Al) HVL: 0.37 mm Cu	1.053	1.040	1.29%
SARRP HVL: 0.66 mm Cu	1.066	1.060	0.54%
X320 HVL: 3.86 mm Cu	1.107	1.106	0.08%

Figure 4 shows the full backscatter factor simulated at different square field sizes and an SSD of 50 cm compared with the value from TG61 table. Note that the field diameter used in TG61 was already converted to square field size. There is excellent agreement between our MC and the TG61 table for X225(Cu). For X225(Al) there is around 1% difference near field size of 10cm but very good agreement elsewhere. For SARRP, the agreement is excellent at small field sizes but the difference grows to around 2% at field size of 20cm. The agreement for X320 is poorer, likely due to fact that the TG61 table around that HVL was created with filtered 280 kVp beam as well as mono-energetic 200 keV beam(Grosswendt, 1993, 1990), which are very different from the Thoraeus filtered 320 kVp beam. Overall, the agreements are very good, showing that our MC simulation settings and setups were reasonable.

The depth dose curves for Figure 2c setup is generated for X225(Cu) (Figure 5) and X225(Al) filter (Figure 6). The dose has been normalized with the water kerma at isocenter. The value at depth = 0 is the backscatter factor $B_w'(T)$ as defined in equation 5. For simplicity, only the field size of [20 cm, 10 cm, 3 cm, 1 cm], and the water phantom thickness of [4 mm, 8 mm, 24 mm, 64 mm, 412 mm] were plotted. For complete results, please refer to the PDD tables in Appendix A. Clearly, as the water thickness decreases, the dose also decreases due to the reduced contribution from phantom backscatter. This effect is also affected by the field size. For 20 cm field size, the dose can vary by around 50% as the water thickness changes. While at 1 cm field size, the impact of the water thickness is only a few percent.

Since the depth dose curves for SARRP and X320 beams exhibit similar behavior as X225 beams, we choose not to generate separate figures for them. The detailed depth dose relation of both beams is listed in Appendix A. Only the depth dose for the water thicknesses of 41.2 cm and 2.4 cm with 20 cm field size are shown in Figure 7 to demonstrate the effect of beam qualities on the depth dose curve. Under the full backscatter condition (41.2 cm water thickness), the differences in beam quality are clearly reflected in the depth dose curve. SARRP, with HVL between the X225(Cu) and X225(Al), has the PDD curve between the X225 beams. In addition, the HVL difference between X225(Cu) and X225(Al) brings 10% difference in PDD curves at full scatter condition. However, the difference quickly reduced as the water thickness reduces. The X320, being on a much higher energy, exhibit a different depth dose curve than the other 3 beam, with lower surface dose and a slower dose fall-off.

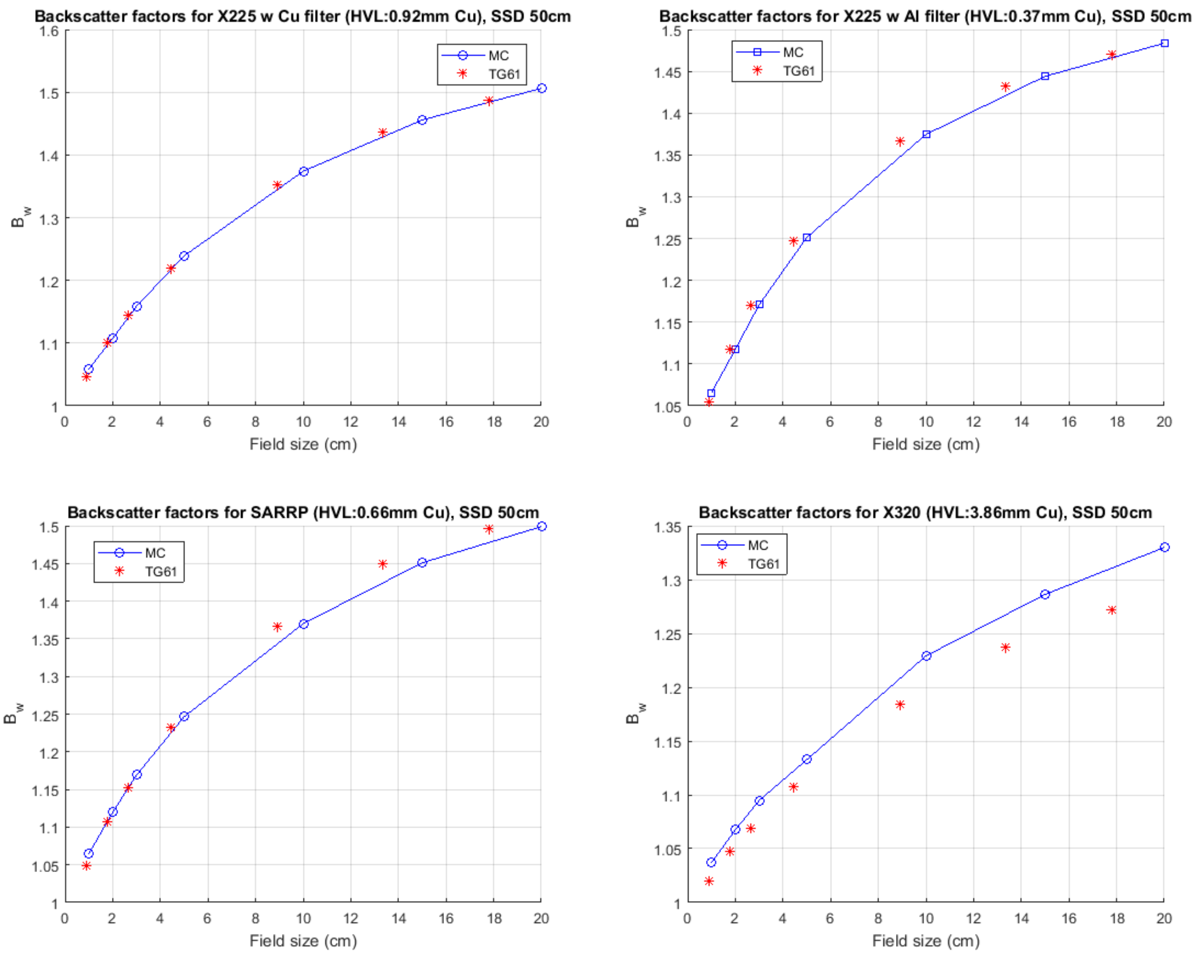

Figure 4. Comparison of the full backscatter factor at different square field size and SSD of 50cm from our MC-simulation (line with circle symbols) and from TG61 table look-up using the HVL of the beam (asterisk symbols) with the field diameter converted to equivalent square field size.

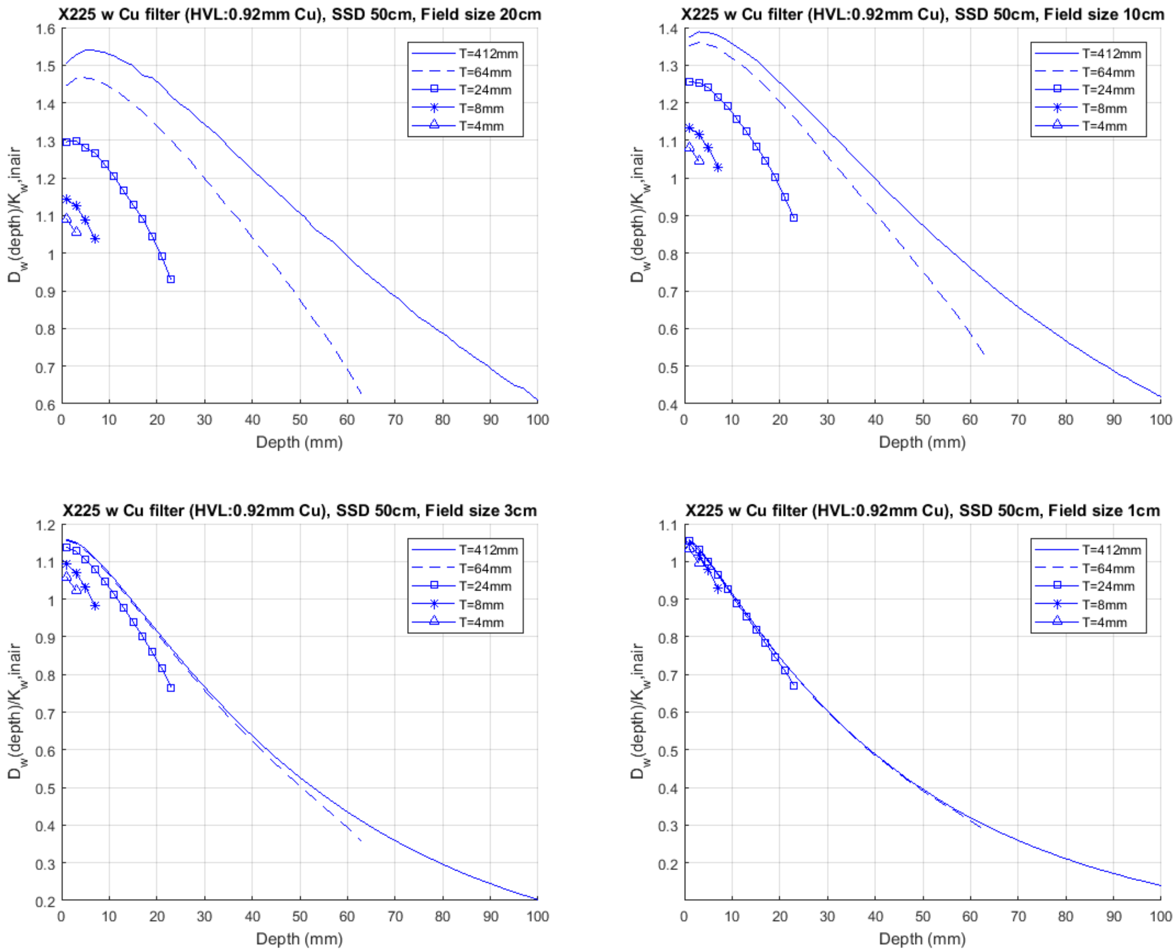

Figure 5. Depth dose curves for different water thicknesses and field sizes for XRAD-225 with Cu filter. Dose is normalized to the water kerma at isocenter.

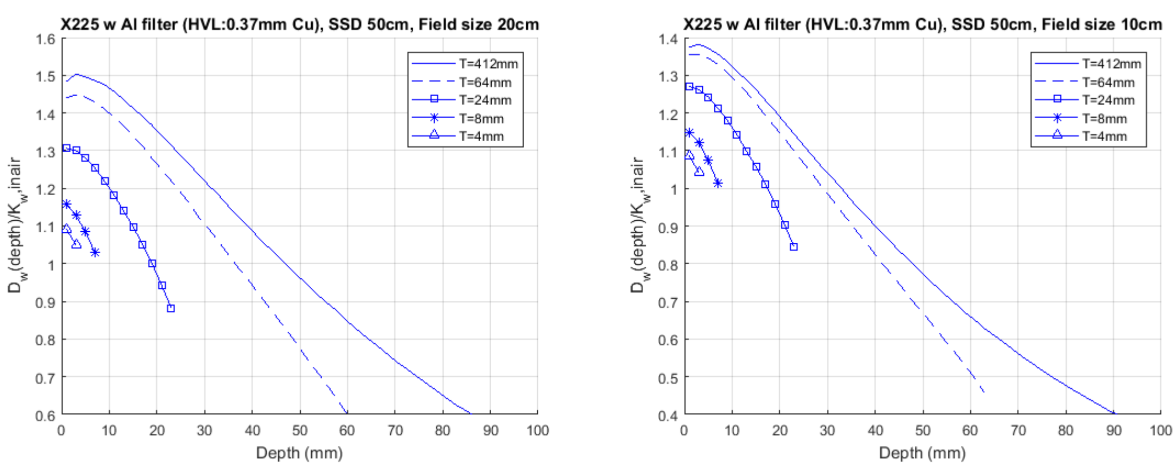

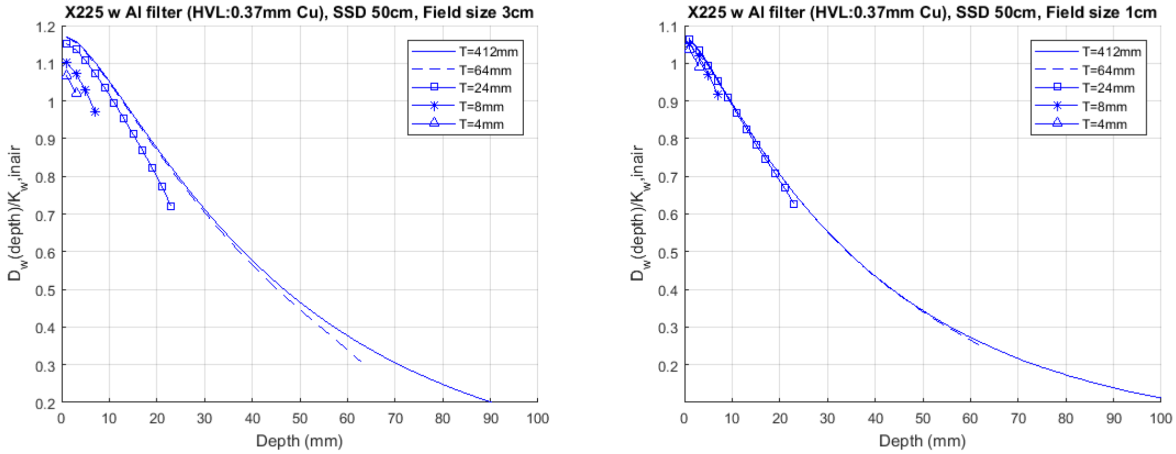

Figure 6. Depth dose curves for different water thicknesses and field sizes for XRAD-225 with Al filter. Dose is normalized to the water kerma at isocenter.

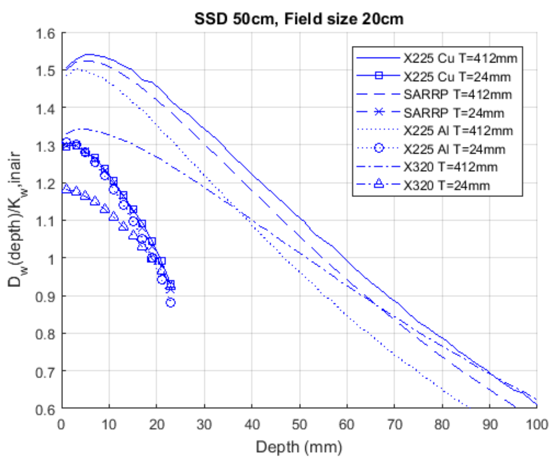

Figure 7. Comparison of Depth dose curves at different beam qualities and water phantom thickness. Solid line: X225 w Cu filter; Dashed line: SARRP; Dotted line: X225 w Al filter; Dash-dot line: X320. Symbols: water thickness of 2.4cm; No symbol: water thickness of 41.2cm.

The impacts of water phantom thickness (*T*) on the backscatter factor $B_w{}'(T)$ at different field sizes can be seen more clearly in Figure 8. Only the X225(Cu) and X225(Al) results are shown. The complete tables for all beam qualities are listed in Appendix B. In addition to the obvious trend that the backscatter increases with the water phantom thickness and field size as Figures 5 and 6 showed, it is worth noting that the water thickness have greater impact on backscatter factor initially but gradually saturates as the thickness is increased. The saturated $B_w{}'(T)$ is the full backscatter factor B_w. For field size of 20 cm, the saturating water thickness is around 20 cm. As field size is smaller, the thickness required for full backscatter decreased accordingly. It seems that the field size is a good rule of thumb value when estimating how much material is needed to establish full backscatter condition. It showed that the maximum thickness used in the simulation (41.2 cm) provides enough backscatter for all field sizes.

Despite the difference in HVL, the shapes of backscatter factor $B_w{}'(T)$ curves for two of the X225 beam qualities look similar, only the full backscatter factor at large water thickness differ. We hypothesized that the $B_w{}'(T)$ of one beam quality *Q2* can be converted to another beam quality *Q1* through:

$$B_{w,Q1}{}'(T) = B_{w,Q2}{}'(T)^{B_{w,Q1}/B_{w,Q2}} \quad . \tag{7}$$

Figure 9 shows the backscatter factor $B_w{}'(T)$ for X225(Cu) beam quality as well as the same factor obtained from rescaling the $B_w{}'(T)$ curves for X225(Al) beam using Eqn. 7. The agreements are very good except for large field size at small water thickness where 3% errors are observed.

The depth dose curves for Figure 3 geometries using X225(Cu) beam are shown on Figure 10. As the figure shows, the variations in radiation setup can have significant impact to dose. At field size of 20 cm, a 4 mm stainless steel below the 2.4cm water phantom can increase the dose in the -12 mm to 0 mm region by 5%. The 0.03 g/cm^3 polyurethane foam, while very low density, can still provide enough backscatter to boost the dose by 2% when it is 20 cm thick. On the other hand, when the 30×30×1.2 cm square water block was replaced with a 10cm diameter × 1.2 cm thick cell dish, the dose was decreased by 4%. And when the 10 cm diameter dish was replaced with 6 cm and then to 3.5 cm, the dose dropped further by 4% and 5% accordingly. Note the dose decrease is not limited to the cell dish (-12 mm to 0 mm region), it also extended to the supporting board (0 mm to 12 mm region) but with slightly reduced magnitude. The dependency on setup conditions is less pronounced when field size was reduced to 5 cm. The impact of 4 mm stainless steel became 1%-2.5% in the -12 mm-0 mm region. The polyurethane foam had negligible effect. The use of cell dish diameter of 10 cm and 6 cm also had negligible effect. Only when we switch to cell dish diameter of 3.5 cm, which is smaller than the radiation field size, showed a 4% decrease in dose.

The simulations for Figure 3 geometries were performed at radiation source to the surface of supporting board at 50cm, which put the SSD of the experimental setup at 48.8cm. The dose profiles obtained at 50cm SSD (Figure 5) has been converted to 48.8cm SSD using the inverse square relation shown as the dashed curve in Figure 10. It matched with the direct simulation at 48.8cm SSD very well.

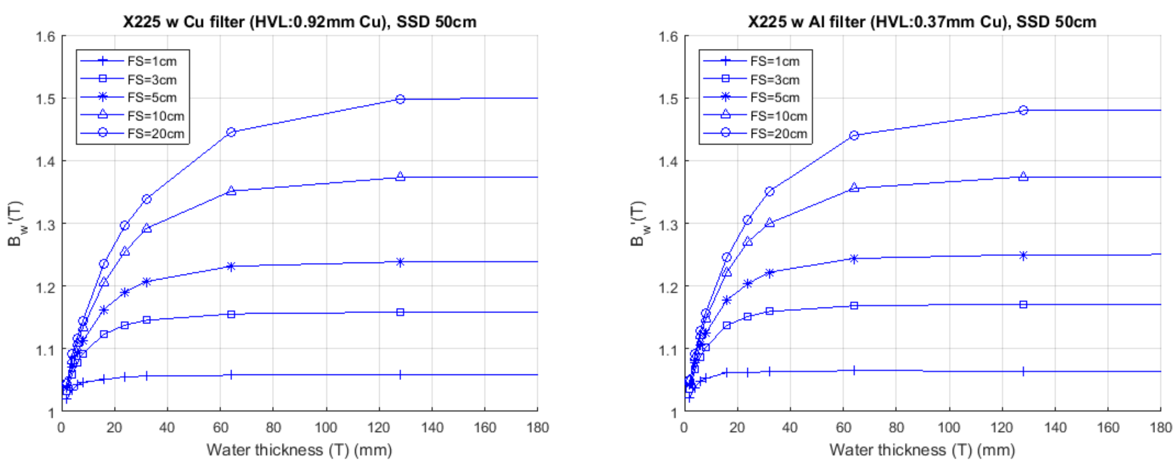

Figure 8. The backscatter factor $B_w{}'(T)$ at field sizes of 1cm, 3cm, 5cm, 10cm and 20cm for X225(Cu) and X225(Al).

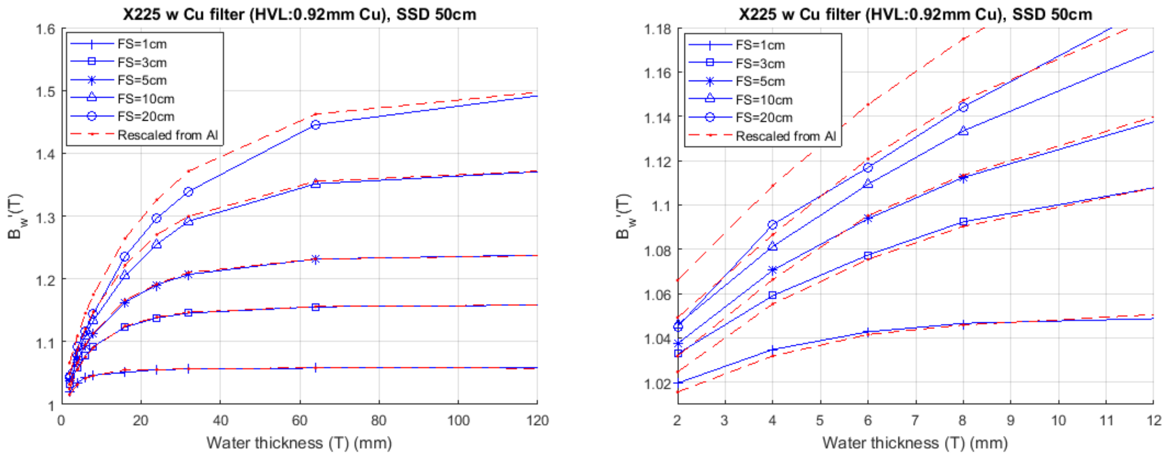

Figure 9. Comparison of the shape of backscatter factor $B_w{}'(T)$ under different beam qualities. The solid line and symbol shows the $B_w{}'(T)$ for X225(Cu), the dashed line shows the $B_w{}'(T)$ for X225(Al) rescaled with a $B_{w,Cu}/B_{w,Al}$ factor. Left shows the comparison at water thickness range of 0 – 120 mm, right is the zoomed in view showing the comparison in the 2-12 mm range.

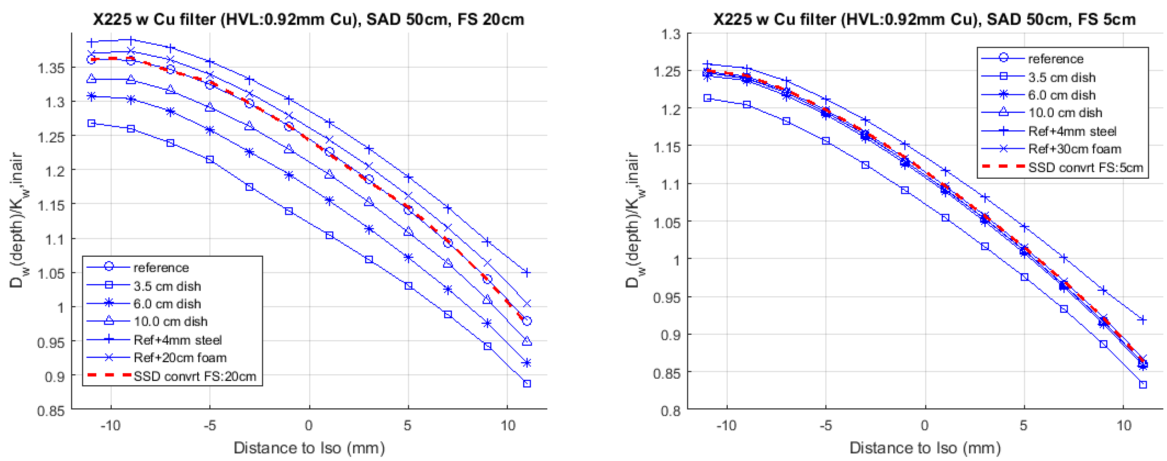

Figure 10. Depth dose curves for Figure 3 geometries. The SSD is 48.8cm (SAD is 50.0cm). Depth doses are plotted from -1.2cm to 1.2cm around isocenter only. Left plot shows the result from field size of 20 cm, right plot shows the result from field size of 5 cm. Dashed curve is the depth dose curve for a 2.4cm thickness water phantom at 50.0cm SSD converted to 48.8cm SSD.

Discussion

The dose for orthovoltage X-ray unit is strongly affected by the thickness of the phantom. This behavior is different from the megavoltage (MV) X-ray that most of the therapist physicists are familiar with. While phantom scatter contributes significantly to dose at both energies, the scattering at MV is dominantly forward whereas there are significant backscattering contributions in orthovoltage range. Therefore, the dose in a phantom for MV beam depends primarily on the phantom material thickness before the point (depth) whereas for orthovoltage beam it depends on both the depth and the thickness of the material after the point (thickness – depth). This behavior can be clearly seen in the depth dose curves in Figure 5 and Figure 6, where the curve for 64 mm thickness phantom closely follows the curve for 412 mm thickness phantom until the last a few centimeter when there is insufficient material to provide phantom backscatter.

For the orthovoltage beam qualities studied, the forward scatter is also significant. This is indicated by the slight build-up section in the depth dose profile at field size of 20cm and phantom thickness of 41.2cm. In addition, the dose in a 3.5cm dish is smaller than the dose at reference condition illustrated in Figure 10 is due to the same reason. If the dose mainly comes from backscatter, then dose in the 3.5cm dish should be higher because the backscatter from the region outside of the 3.5cm dish is higher than in the reference condition.

Understanding and quantifying the impact of the material thickness on the dose is very important in ensuring the dosimetric accuracy of the orthovoltage X-ray unit. Following TG-61's calibration procedure, the dose to water under the full backscattering condition of an orthovoltage X-ray unit can be determined. However, the conditions where the cell or animal irradiations were performed are almost never in the full scatter condition, except when very small field sizes were used. Our simulation showed that there can be as much as 40-50% dose errors if one wrongfully uses the calibrated dose to water from TG-61 when the full scatter condition is far from met (e.g. the surface dose on a 4mm support board).

Radiochromic film, as well as other dosimeters like OSLD, TLD, has also been used for the radiobiology irradiator dosimetry (Deng *et al.*, 2007; Rodriguez *et al.*, 2009). However, due to the energy dependent response of these dosimeters, a calibration factor has to be determined for the energy of interest. Common approach is to deliver a fixed amount of radiation to the dosimeter and establish the relation between the responses to the known doses delivered, which is determined through TG-61 assuming full backscatter. It is important to ensure the full backscattering condition is met for the calibration irradiation. Based on the backscatter factor $B_w{}'(T)$ curves on Figure 8, it is recommended to use small field sizes between 1cm to 3cm and at least 4cm solid water as backscattering material to generate calibration curve.

Similar caution has to be applied when one tries to estimate dose for an experiment setup from the doses measured with TG-61 in-water measurement. Precision X-ray Inc. provides a 20cm diameter measuring cup-like container (Part No: XD1610-0100) with ion chamber at 2cm from the bottom for output and PDD measurement. One should note that this 2cm to bottom distance is not enough to provide full backscatter. Even the 6 cm phantom used by Azimi et al.(Azimi *et al.*, 2015) as backscatter is likely still underestimating the dose at full scatter condition by 5% at 20cm field size, according to our simulation of PDD curves for 6.4cm vs 41.2cm water phantom thickness. Therefore, it is strongly recommended that the depth dose table in Appendix A be consulted to ensure the correct calibration and extensions to other backscatter conditions in experiments.

Although Appendix A only lists the depth dose table for a 50cm SSD, the dose at other SSD can be computed through inverse square law. Note that this assumes that the field sizes at each depth for the two SSDs are equal. When the SSD change is big that the assumption does not hold, when can still perform the inverse square law correction and then estimating the residue error from the backscatter factor $B_w'(T)$ table (Appendix B) by plugging in the backscatter thickness from the point of interest, and the field size difference at the point of interest.

TG-61 created lookup tables for 36 beam qualities. In this study, we only have 4. However, the good match in Figure 9 shows that for beam qualities slightly different from the four studied, Eqn. 7 can provide a very good approximation for the backscatter factor at a given backscatter water phantom thickness.

Most radiobiology experiments setups are obviously more complex than simple water blocks. The depth dose plots in Figure 10 illustrated that the depth dose curves for simple geometries illustrated in Figure 2c cannot be blindly used for experimental setups. Ideally, one should either use a comprehensive TPS that accurately models this complex dosimetry behavior in orthovoltage range, or perform an accurate measurement for each experimental setup. In the absence of both, a general recommendation is to reduce the field size used so that the backscatter condition would have less impact. For the same 3.5 cm dish, reducing the field size from 20cm to 5cm, while still maintains the coverage of the entire dish, reduces the dose error from 12.5% to 5% before any correction is applied. The dose error can be reduced further if 3.5 cm field size is used, and/or if a correction is estimated from Figure 10.

Conclusions

MC simulation was used to study the impact of the backscatter water phantom thickness on the depth dose profile for two commercially available radiobiology X-ray irradiators on the market (Xstrahl SARRP and Precision X-RAD). Dose at the orthovoltage energies commonly used in radiobiology research is sensitive to the amount of backscatter material and other differences in setup (such as the size of cell dish used). At field size of 20 cm, as much as 50% dose difference can be made for different backscatter thicknesses. The magnitude of impact decreases with the decrease of field size. The backscatter thickness needed to provide full backscatter roughly equals to the square field size used. It is very important to either ensure the full backscatter condition during system calibration and dosimeter calibration by providing enough backscatter material and use small field size or lookup the depth dose table and backscatter factor table in Appendix for correction factors.

Acknowledgments

We would like to thank Dr. Peter Kazanzides from the Johns Hopkins for kindly providing the spectrum for SARRP, and Dr. Paul DeJean from Precision X-Ray Inc. for kindly providing the spectrum for XRAD systems.

References

Azimi R, Alaei P, Spezi E and Hui S K 2015 Characterization of an orthovoltage biological irradiator used for radiobiological research *Journal of radiation research* **56** 485-92

Bazalova M, Nelson G, Noll J M and Graves E E 2014 Modality comparison for small animal radiotherapy: A simulation study *Medical physics* **41**

Bazalova M, Zhou H, Keall P J and Graves E E 2009 Kilovoltage beam Monte Carlo dose calculations in submillimeter voxels for small animal radiotherapy *Medical physics* **36** 4991-9

Brahme A 1984 Dosimetric precision requirements in radiation therapy *Acta Radiologica: Oncology* **23** 379-91

Chica U, Anguiano M and Lallena A 2009 Benchmark of PENELOPE for low and medium energy X-rays *Physica Medica* **25** 51-7

Cho N, Tsiamas P, Velarde E, Tryggestad E, Jacques R, Berbeco R, McNutt T, Kazanzides P and Wong J 2018 Validation of GPU‐accelerated superposition‐convolution dose computations for the Small Animal Radiation Research Platform *Medical physics* **45** 2252-65

Deng H, Kennedy C W, Armour E, Tryggestad E, Ford E, McNutt T, Jiang L and Wong J 2007 The small-animal radiation research platform (SARRP): dosimetry of a focused lens system *Physics in Medicine & Biology* **52** 2729

Desrosiers M, DeWerd L, Deye J, Lindsay P, Murphy M K, Mitch M, Macchiarini F, Stojadinovic S and Stone H 2013 The importance of dosimetry standardization in radiobiology *Journal of research of the National Institute of Standards and Technology* **118** 403

Grosswendt B 1990 Dependence of the photon backscatter factor for water on source-to-phantom distance and irradiation field size *Physics in Medicine & Biology* **35** 1233

Grosswendt B 1993 Dependence of the photon backscatter factor for water on irradiation field size and source-to-phantom distances between 1.5 and 10 cm *Physics in Medicine & Biology* **38** 305

Jacques R, Smith D, Tryggestad E, Wong J, Taylor R and McNutt T *Proc. ICCR,2010),* vol. Series 2010*)*: Citeseer) pp 2-5

Jaffray D A *Seminars in Radiation Oncology,2007),* vol. Series 17*)*: Elsevier) pp 243-4

Kavanagh B D, Pan C C, Dawson L A, Das S K, Li X A, Ten Haken R K and Miften M 2010 Radiation dose–volume effects in the stomach and small bowel *International Journal of Radiation Oncology* Biology* Physics* **76** S101-S7

Kirkpatrick J P, van der Kogel A J and Schultheiss T E 2010 Radiation dose–volume effects in the spinal cord *International Journal of Radiation Oncology* Biology* Physics* **76** S42-S9

Ma C M, Coffey C, DeWerd L, Liu C, Nath R, Seltzer S and Seuntjens J 2001 AAPM protocol for 40 ‐ 300 kV x ‐ ray beam dosimetry in radiotherapy and radiobiology *Medical physics* **28** 868-93

Marks L B, Bentzen S M, Deasy J O, Bradley J D, Vogelius I S, El Naqa I, Hubbs J L, Lebesque J V, Timmerman R D and Martel M K 2010 Radiation dose–volume effects in the lung *International Journal of Radiation Oncology* Biology* Physics* **76** S70-S6

Pedersen K H, Kunugi K A, Hammer C G, Culberson W S and DeWerd L A 2016 Radiation biology irradiator dose verification survey *Radiation research* **185** 163-8

Podgorsak E B 2005 External photon beams: Physical aspects *Radiation Oncology Physics: A handbook for teachers and students'. Vienna: IAEA* 169

Robbins M E 2011 Biodosimetry Bloppers: Why Radiation Biology Needs Radiation Physics.

Rodriguez M, Zhou H, Keall P and Graves E 2009 Commissioning of a novel microCT/RT system for small animal conformal radiotherapy *Physics in Medicine & Biology* **54** 3727

Salvat F, Fernάndez-Varea J M and Sempau J *Workshop proceedings,2006),* vol. Series 4*)*: Nuclear Energy Agency, Organization for Economic Co ‐ operation and Development Barcelona, Spain)

Sempau J, Sanchez-Reyes A, Salvat F, ben Tahar H O, Jiang S and Fernández-Varea J 2001 Monte Carlo simulation of electron beams from an accelerator head using PENELOPE *Physics in Medicine & Biology* **46** 1163

Sterpin E, Sorriaux J and Vynckier S 2013 Extension of PENELOPE to protons: simulation of nuclear reactions and benchmark with Geant4 *Medical physics* **40**

Van Dyk J, Keane T, Kan S, Rider W and Fryer C 1981 Radiation pneumonitis following large single dose irradiation: a re-evaluation based on absolute dose to lung *International Journal of Radiation Oncology• Biology• Physics* **7** 461-7

van Hoof S J, Granton P V and Verhaegen F 2013 Development and validation of a treatment planning system for small animal radiotherapy: SmART-Plan *Radiotherapy and Oncology* **109** 361-6

Verhaegen F, Granton P and Tryggestad E 2011 Small animal radiotherapy research platforms *Physics in Medicine & Biology* **56** R55

Verhaegen F and Seuntjens J 2003 Monte Carlo modelling of external radiotherapy photon beams *Physics in medicine & biology* **48** R107

Wong J, Armour E, Kazanzides P, Iordachita I, Tryggestad E, Deng H, Matinfar M, Kennedy C, Liu Z and Chan T 2008 High-resolution, small animal radiation research platform with x-ray tomographic guidance capabilities *International Journal of Radiation Oncology* Biology* Physics* **71** 1591-9

Ye S-J, Brezovich I A, Pareek P and Naqvi S A 2004 Benchmark of PENELOPE code for low-energy photon transport: dose comparisons with MCNP4 and EGS4 *Physics in Medicine & Biology* **49** 387

Yoshizumi T, Brady S L, Robbins M E and Bourland J D 2011 Specific issues in small animal dosimetry and irradiator calibration *International journal of radiation biology* **87** 1001-10